ingegneria sismica
International Journal of Earthquake Engineering
Anno XLIII - Num. 1 - 2026

Quantitative analysis of the influence of stiffness matrix on structural stability in tensegrity design

Yingyu Zhao[1,*], *Ani Luo*[1] *and Heping Liu*[1]

[1] College of Mechanical and Electrical Engineering, Harbin Engineering University, Harbin 150001, China

SUMMARY: *This paper presents a quantitative framework oriented to computer analysis for evaluating the influence of stiffness matrix properties on the stability of tensegrity structures during structural design. A data set containing 3600 configuration samples is generated around the component topology, prestress level, node coordinates, material parameters and boundary conditions. The global stiffness matrix is calculated for each set of samples, and statistics such as eigenvalue distribution, condition number, energy curvature, modal sensitivity, and geometric coupling are extracted. Subsequently, graph-aided regression and classification modules are constructed to estimate the stability margins and identify stable, critical and unstable states under different load paths. The experimental results show that the proposed framework achieves 95.4% classification accuracy and 0.918 F1 value in steady state recognition, the mean absolute error of stability margin prediction is 0.037, and the inference time for a single sample is 0.42s. The research results provide a computable basis for the design of tensegrity structures considering stability in engineering, and reflect a relatively stable engineering adaptability and screening ability.*

KEYWORDS: *Tensegrity; Stiffness matrix; Structural stability; Intelligent computing*

1 Introduction

With the development of lightweight spatial structures and deployable systems, tensegrity structures have become an important object in structural design due to their flexible configuration and high material utilization. This kind of structure is composed of compressive members, cable members and joint elements. The overall stability of the structure is not only determined by the strength of the member, but also depends on the topological connection, prestress distribution, geometric shape and spectral characteristics of the stiffness matrix. The establishment of a computable and comparable quantitative stability analysis method around the stiffness matrix has become the basis for accurate modeling and intelligent discrimination of tensegrity design.

Ma et al. studied the dynamics and control process of clustered tensegrity systems and revealed the coupling relationship between structural response and state regulation [1]. Lee et al. proposed a deep neural network method for tensegrity form finding, which makes the mapping calculation of complex configurations with data-driven characteristics [2]. Koohestani studied the topological and geometric modeling of multi-frequency geodesic icosahedral tensegrity, which provided an expression for the parametric organization of complex regular structures [3]. Bel Hadj Ali et al. established the finite element formula of

*zhaoyingyu@hrbeu.edu.cn
https://doi.org/10.65102/is2026304
Published: 30 April, 2026

cluster cables considering slip friction effect, which enriched the basis for nonlinear solution of cable elements [4]. Song et al. studied the form-finding process of concatenated tensegrity and explained the connection between geometric generation and stable state [5]. Xu et al. proposed a two-step topology solution method combining mixed integer programming and nonlinear programming to make the topology search process more controllable [6]. Fernandez-Ruiz et al. studied the topological design of octahedral tensegrity, which provided a geometric basis for structural organization under regular unit expansion [7]. Trinh et al. proposed a neural network prestress design method combined with force density information, which improved the parameter identification ability under multiple self-stress modes [8]. Zhang et al. studied the self-equilibrium solution method considering the zero stress state and the construction process, which provided reference for the formation analysis of the prestressed system [9].

Obara et al. studied the dynamic stability of tensegrity under dead load and revealed the influence of external load form on the stability boundary [10]. Chen et al. studied the minimum mass design of clustered tenseholics, showing that there is a correlation between mass configuration and equivalent stiffness [11]. Chen et al. further analyzed the cable driving strategy of V-Expander tensetuality, and showed that the driving path would change the response mode of the system [12]. Ge et al. proposed a probabilistic computing framework based on machine learning to characterize the uncertainty propagation in the tensegrity driving process [13]. Kumar et al. studied the tensegrity bridge form finding method supported by genetic algorithm, which enhanced the computational search ability in complex design space [14]. Luo et al. directly studied the stiffness characteristics of three-bar tensegrity and showed that the stiffness matrix expression plays a central role in stability analysis [15]. Feng et al. proposed a fast model predictive control strategy for tensegrity vibration control, which reflects the fusion trend of structural analysis and algorithm calculation [16].

Wang et al. studied a unified analysis method for general tensegrity self-balance, mechanism stiffness and self-stress, which improved the theoretical basis for stability discrimination [17]. Xu et al. proposed a generalized objective function based on weight coefficient to solve the tensegrity topology, which extended the multi-index joint calculation path [18]. Liu et al. studied an efficient form-finding method under resource constraints, which improved the compactness and efficiency of the solution process [19]. Wang et al. studied active tensegrity topology optimization, which provided a path for configuration update and stable co-design [20]. Existing research has covered many aspects such as shape finding, topology design, prestress configuration, dynamic response and optimal control. However, in the structural design stage, how to convert the feature information in the stiffness matrix into calculation variables that can be used for quantitative stability comparison and further incorporated into the data analysis process still needs a systematic organization.

Based on this, in this paper, parametric modeling, data mapping, stiffness matrix generation, feature extraction and intelligent analysis are connected as a continuous computing link. The sample representation is constructed based on node coordinates, cable properties, topological relationships and prestress inputs. The stability level recognition and stability margin prediction are realized by combining classification and regression calculation, so as to provide quantitative basis for computer analysis for tensegrity design.

2 Basic theory and technical framework

2.1 Principle of parametric modeling and stiffness matrix representation of tensegrity structures

In the parametric modeling of tensetic integral structures, the spatial shape is not directly input into the calculation program, but the nodes, bars, cables, boundary constraints, prestress levels and load paths are uniformly translated into computable data objects. In this paper, the modeling path of "topological index-geometric mapping-element generation-matrix assembly-feature cache" is adopted to write the shape information, material information and force information in structural design into the same data domain. The node coordinates are saved as a three-dimensional array, and the rod-cable connection relationship is expressed as a weighted adjacency list. The component category, section parameters, elastic modulus, density and initial cable force are written into the attribute vector, and then the degree of freedom expansion and unit direction recognition are completed by the program. After this treatment, different configurations, different prestress levels, and different support modes can enter the stiffness matrix calculation process under a unified framework, providing continuous input for subsequent stability measures.

Fig. 1 shows the parametric modeling and stiffness matrix representation process adopted in this section. The parameter input layer at the left end of the figure includes node coordinates, rod and cable topology, material properties, constraint mode and prestress level. The structure generation layer in the middle completes topology coding, geometric mapping, unit classification, local coordinate establishment and degree of freedom numbering in turn. The matrix calculation layer on the right continues to complete the local stiffness construction, geometric stiffness correction, global assembly and feature caching. The key of this process is that the structure graph does not directly enter the stability analysis, but is first transformed into an indexable, traversable and updatable matrix object, and then the eigenvalue spectrum, condition number, modal sensitivity and coupling index are output by the matrix feature extraction module. The arrow lines in the figure reflect the unidirectional transmission of design parameters to calculation results and the reverse check relationship between matrix statistics and design variables. Therefore, the figure not only describes the modeling sequence, but also illustrates the logical closed loop between structure design, matrix generation and stability representation.

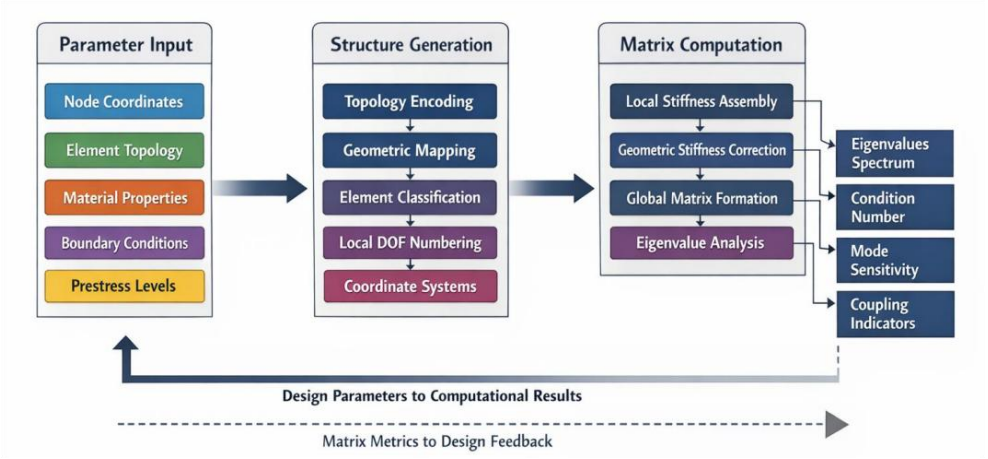

Figure 1: Flowchart of parametric modeling and stiffness matrix representation of tensegrity structures

In the computer implementation, tensegrity structures are expressed as heterogeneous graphs with attributes. Each node has a unique number and coordinate state. Each edge records the component type, starting and ending nodes, geometric length and initial value of prestress at the same time, and the program generates local coordinate system, direction cosine and degree of freedom mapping table. The expression can directly synchronize the structural shape changes to the matrix assembly link, so that the structural design is no longer static graphics generation, but an updatable object oriented to calculation and analysis. In order to ensure data consistency between different design samples, this paper sets configuration labels, constraint labels and load labels, and encapsulates them as standard input tensors to support batch sample calculation and subsequent intelligent discrimination calls.

In order to compress the set of nodes, connection sets, material parameters, prestress variables and boundary states involved in the design phase of tensetility structure into a structured object that can be directly called by the program, this paper firstly constructs the overall parametric description as follows:

$$\mathcal{S} = (\mathcal{V}, \mathcal{E}, \mathrm{X}, \mathrm{U}, \mathrm{M}, \mathrm{P}, \mathrm{C}), \quad \mathrm{U} = \psi(\mathrm{X}, \mathcal{E}), \quad \mathrm{C} = \chi(\mathcal{E}, \mathrm{M}, \mathrm{P}) \tag{1}$$

where $\mathcal{V}$ represents the node set, $\mathcal{E}$ represents the connection set, X represents the node coordinate matrix, U represents the unit direction and length set generated by geometric relationship, M represents the material and section parameter set, P represents the prestressed parameter set, C represents the boundary constraint and load configuration set, $\psi(\cdot)$ and $\chi(\cdot)$ represent the geometric mapping function and constraint encoding function respectively. In Equation (1), the discrete structure objects are sorted into uniform data containers, so that the subsequent matrix assembly has a consistent data entry.

In order for the program to generate the length, direction cosine, and axial projection matrices simultaneously as it traverses each rod-cable element, the element geometry and its projection relationship are written as follows:

$$\mathrm{d_e} = \mathrm{x_j} - \mathrm{x_i}, \quad \mathrm{L_e} = (\mathrm{d_e^T d_e})^{1/2}, \quad \mathrm{q_e} = \frac{\mathrm{d_e}}{\mathrm{L_e}}, \quad \mathrm{P_e} = \mathrm{q_e q_e^T} \tag{2}$$

Here, $\mathrm{d_e}$ represents the direction vector of the e cell, $\mathrm{L_e}$ represents the cell length, $\mathrm{q_e}$ represents the unit direction vector, and $\mathrm{P_e}$ represents the axial projection matrix. Equation (2) is used to determine the orientation of the element in the global coordinate system and provides the basis for the decomposition of the local and geometric stiffness.

In order to make the local stiffness expression reflect both the axial contribution of the material and the geometric contribution induced by the prestress, the element tangent stiffness is constructed as follows:

$$\mathrm{K_e^{loc}} = \frac{\mathrm{E_e A_e}}{\mathrm{L_e}} \begin{bmatrix} 1 & -1 \\ [-2\mathrm{pt}] -1 & 1 \end{bmatrix} \otimes \mathrm{P_e} + \frac{\mathrm{T_e^0}}{\mathrm{L_e}} \begin{bmatrix} 1 & -1 \\ [-2\mathrm{pt}] -1 & 1 \end{bmatrix} \otimes (\mathrm{I_3} - \mathrm{P_e}) \tag{3}$$

Here, $\mathrm{E_e}$ represents the elastic modulus, $\mathrm{A_e}$ represents the cross-sectional area, $\mathrm{T_e^0}$ represents the initial prestress of the element, $\mathrm{I_3}$ represents the third-order identity matrix, and $\otimes$ represents the Kronecker product. In Equation (3), the former term describes the axial stiffness of the material, and the latter term describes the geometric correction caused by the prestress, so the local stiffness matrix can more completely reflect the stress basis of the tensegrity structure.

Considering that the components in the tensegrity structure have different spatial orientations and node coupling states, the local stiffness also needs to be projected into the

global coordinate system through direction transformation and additional correction, and its mapping relationship is written as follows.

$$K_e^{glob} = R_e^T K_e^{loc} R_e + \omega_e H_e^T H_e \tag{4}$$

Here, R_e represents the direction transformation matrix from local to global, H_e represents the additional coupling matrix of nodes, and ω_e represents the coupling weight. Equation (4) not only completes the coordinate transformation, but also incorporates the node rotation Angle coupling and additional configuration correction into the overall expression, making the matrix representation closer to the actual structure state.

When all the cable elements are traversed, the program adds the stiffness of each element to the overall stiffness system according to the degree of freedom assembly matrix, and writes the supporting constraint in the form of penalty term. The overall assembly expression is as follows:

$$K = \sum_{e=1}^{m} B_e^T K_e^{glob} B_e + \mu D^T D \tag{5}$$

Here, m represents the total number of cells, B_e represents the degree of freedom mapping matrix of the e cell, D represents the constraint matrix, and μ represents the constraint penalty coefficient. Equation (5) translates the discrete components into a unified global stiffness matrix, and ensures that the boundary conditions are consistent at the matrix level.

In order to make the stiffness matrix not only assume the function of response solving, but also directly serve the subsequent stability identification and quantitative comparison, this paper further extracts spectral statistics, coupling statistics and sparse statistics, and organize them into a unified feature vector, which is expressed as follows:

$$z = \left[\lambda_{min}^{+}, \kappa(K), \mathrm{tr}(K), \frac{\sum_{i=1}^{r}\lambda_i}{\sum_{j=1}^{n}\lambda_j}, \rho(K), \|K - K^T\|_F\right]^T, \quad s = \sigma(w^T z + b) \tag{6}$$

Here, λ_{min}^{+} represents the smallest positive eigenvalue, $\kappa(K)$, represents the condition number, $\mathrm{tr}(K)$ represents the trace, $\rho(K)$ represents the nonzero element density, $\|\cdot\|_F$ represents the Frobenius norm, w and b are computational parameters, $\sigma(\cdot)$ is the output mapping function, and s represents the stability characterization value. Equation (6) shows that the stiffness matrix can form a unified input after feature extraction, so that the matrix objects in the structural design stage can be directly transformed into quantitative features that can be called by subsequent modules.

The above modeling and characterization process shows that the parametric modeling of tensegrity is not a preprocessing step independent of stability analysis, but the starting point of the whole quantitative analysis link. By translating the structural design variables into matrix objects, and then translating the matrix objects into comparable and learnable features, the stability discrimination, margin prediction and scheme selection in the subsequent chapters have a consistent data foundation. Meanwhile, the parameter input, matrix generation and feature caching are implemented in a hierarchical way, and the existing data structure is not destroyed by geometric update, and the whole historical samples need not be assembled repeatedly for local unit recalc - ation. This mechanism provides a stable interface for large-scale sample training, sensitivity scanning and fast design iteration. On this basis, the

matrix representation also retains three types of information granularity: node level, component level and global level, which can not only support the location of local instability sensitive areas, but also support the unified comparison of global stability levels. It can be seen that the framework has clear engineering practicability and stable expansion ability.

2.2 Structural stability criterion and numerical calculation theory

The stability determination of tensegrity structures is not equivalent to the stiffness checking of conventional bar structures. Since these systems rely on prestress to form a self-equilibrium state, configuration disturbance, constraint variation and local stiffness attenuation will directly change the matrix spectral distribution. Therefore, the stability criterion should simultaneously describe the balance maintaining ability, the displacement amplification tendency and the critical instability sensitivity. Based on the parametric modeling in the previous section, the global stiffness matrix, tangent stiffness matrix and disturbance response vector are integrated into the numerical analysis link, and eigenvalue evolution, energy curvature and residual convergence are used as the three core criteria to establish the stability calculation framework suitable for the tensegrity design stage.

In the computer implementation, the stability analysis module does not directly make a static judgment of a single load step, but organizes the load increment, prestress correction and boundary disturbance into a continuous state sequence. The program first reads the global matrix and constraint matrix, then updates the tangent matrix according to the load path, and obtains the critical index through the process of spectral decomposition and iterative balance. This process avoids the one-sidedness of judging the stability only by the single-step displacement value, and also enables the horizontal comparison of different design samples under the same numerical scale. In order to ensure the callability of subsequent intelligent analysis, this paper synchronously records the minimum eigenvalue, the second derivative of potential energy, the displacement increment norm and the residual vector norm for each step calculation, and writes them into the stability state buffer, and forms a unified output. And easy to track.

Fig. 2 shows the calculation flow of the structural stability criterion adopted in this paper. In the figure, the input of the left side is the load path, the prestress level and the boundary constraint disturbance. In the middle part, tangent matrix generation, eigenvalue screening, energy curvature evaluation and nonlinear balance iteration are completed in turn. The arrow line indicates that the state variable is passed layer by layer along the calculation link, and the dashed loop indicates that the iterative residual does not meet the threshold to re-enter the matrix correction link. This figure illustrates that the criterion adopted in this section is not used in isolation, but a joint decision mechanism composed of spectral analysis, energy analysis and incremental iteration.

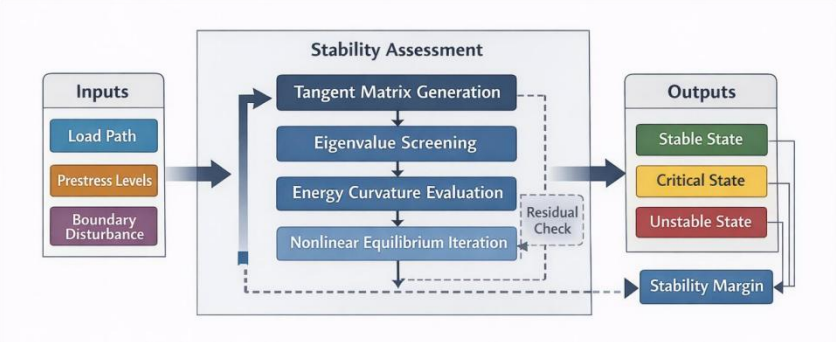

Figure 2: Flowchart for calculating the joint criterion of structural stability

In order to make the equilibrium conditions of the structure in the disturbance state be uniformly written into the solvable equation, the equilibrium relationship under the joint action of external load, prestress and geometric nonlinearity is expressed as follows.

$$r^{(k)} = f_{ext}(\lambda^{(k)}) - f_{int}\left(u^{(k)}, p^{(k)}\right) - C^{T}\eta^{(k)} = 0 \tag{7}$$

Here, $r^{(k)}$ represents the residual vector of the k iteration, $f_{ext}(\lambda^{(k)})$ represents the external load vector under load step parameter $\lambda^{(k)}$, $f_{int}\left(u^{(k)}, p^{(k)}\right)$ represents the internal force vector jointly determined by the displacement vector $u^{(k)}$ and the prestressed state $p^{(k)}$, C is the constraint matrix, and $\eta^{(k)}$ is the constraint reaction force vector. Equation (7) gives the unified expression of nonlinear equilibrium, and each subsequent step of stability determination starts from this residual equation.

Where, the displacement vector in the balance equation is controlled by the load step parameters, and the tangent matrix is composed of the material stiffness, geometric stiffness and constraint correction together. When the incremental load enters, the program updates the state cyclically according to the residual vector and the displacement correction. Such a representation enables tensegrity structures to enter a unified solution framework under different prestress levels, boundary conditions and load paths, and provides a matrix basis for critical state identification.

In order to obtain a convergent displacement correction and suppress numerical oscillations caused by boundary disturbances in the iterative process, the incremental iterative relation with damping correction is adopted as follows.

$$\Delta u^{(k)} = \left(K_t^{(k)} + \alpha C^{T}C\right)^{-1} r^{(k)}, \quad u^{(k+1)} = u^{(k)} + \omega^{(k)}\Delta u^{(k)} \tag{8}$$

Here, $K_t^{(k)}$ represents the tangent stiffness matrix of the k iteration, α is the constraint stabilization coefficient, and $\omega^{(k)}$ is the damping update coefficient. The first half of Equation (8) is used to calculate the displacement increment, and the second half completes the state update. This formula ensures that the numerical process still maintains the stable iteration ability in the critical interval.

Fig. 3 illustrates the iterative update process of the numerical calculation theory in the program. The input terminal first reads the displacement state and the prestress state of the previous load step, and then generates the tangent matrix and the equivalent load vector. The candidate displacement is obtained by incremental solution, and then the residual test and curvature test are used to decide whether to enter the next round of correction. If the residual satisfies the threshold and the minimum eigenvalue remains positive, the current state is denoted as stable. If the smallest eigenvalue is close to zero and the curvature decreases, the program is marked as critical. If the residual is enlarged and the displacement increment is abrupt, it turns into the unstable state. This process ensures that the criterion output is consistent with the actual numerical process.

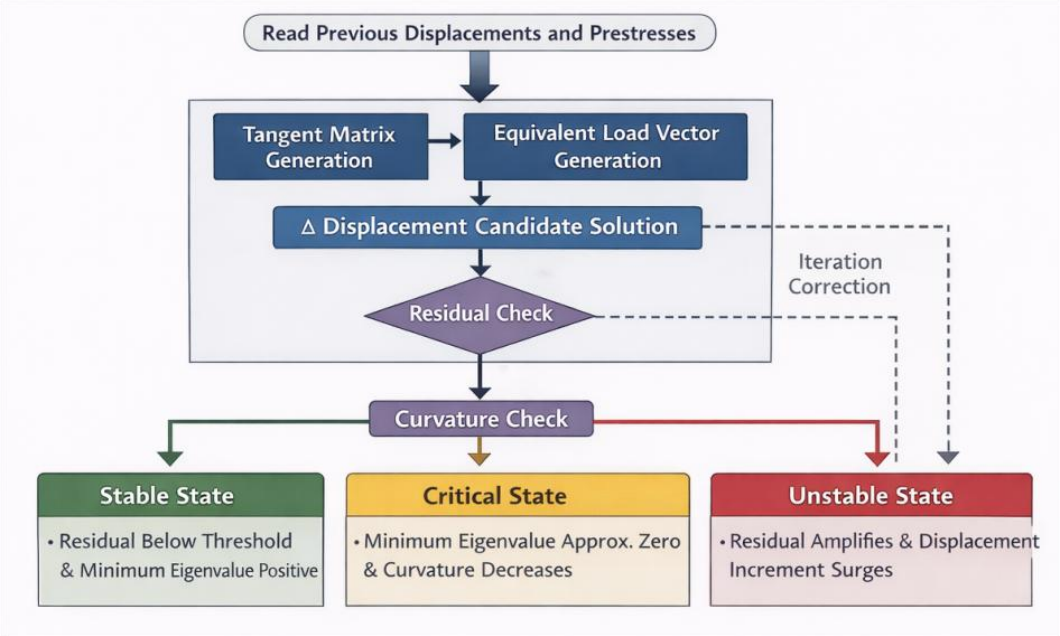

Figure 3: Graph of program iterative update process for numerical computation theory

In order to extract the index that can directly reflect the critical proximity from the matrix spectral change, this paper constructs the generalized eigenvalue relationship between the tangent stiffness matrix and the mass-type measurement matrix as follows.

$$K_t^{(k)}\phi_i^{(k)} = \lambda_i^{(k)} M_s \phi_i^{(k)}, \quad \Lambda_c^{(k)} = \min_{\lambda_i^{(k)}>0} \lambda_i^{(k)} \tag{9}$$

Here, $\phi_i^{(k)}$ is the i eigenvector,$\lambda_i^{(k)}$ is the corresponding eigenvalue, M_s is the stability measure matrix, and $\Lambda_c^{(k)}$ is the minimum positive eigenvalue of the current load step. Equation (9) transforms the structural spectral information into a single critical index, and when Λc(k) continues to decrease and approaches zero, the structure approaches the critical equilibrium boundary.

In the stability measure, a curvature quantity that can reflect the bending degree of potential energy is also needed in addition to the spectral index. Therefore, the energy curvature in the direction of incremental displacement is defined as follows in this paper.

$$\chi^{(k)} = \frac{\left(\Delta u^{(k)}\right)^T K_t^{(k)} \Delta u^{(k)}}{\|\Delta u^{(k)}\|_2^2 + \varepsilon} \tag{10}$$

Here, $\chi^{(k)}$ represents the energy curvature index of the k iteration, and ε is the regularization constant to prevent the denominator from being too small. Equation (10) is used to describe the rate of potential energy change in the incremental direction. When this value decreases significantly, the structure enters the softening interval and the stability margin shrinkates synchronously.

In order to compress the spectrum information, energy information and iteration information into stability representation values that can be directly called by subsequent modules, this paper constructs the comprehensive decision function as follows:

$$S^{(k)} = \sigma\left(\theta_1 \widehat{\Lambda}_c^{(k)} + \theta_2 \hat{\chi}^{(k)} - \theta_3 \hat{\rho}^{(k)} - \theta_4 \hat{v}^{(k)}\right),$$
$$\hat{\rho}^{(k)} = \frac{\left\|r^{(k)}\right\|_2}{\|f_{ext}\|_2 + \varepsilon}, \quad \hat{v}^{(k)} = \frac{\left\|\Delta u^{(k)}\right\|_2}{\|u^{(k)}\|_2 + \varepsilon} \tag{11}$$

Here, $S^{(k)}$ is the comprehensive stability representation value, $\sigma(\cdot)$ is the mapping function, θ_1 to θ_4 are the weight parameters, $\widehat{\Lambda}_c^{(k)}$ and $\hat{\chi}^{(k)}$ represent the normalized spectral index and curvature index, $\hat{\rho}^{(k)}$ represents the normalized residual ratio, and $\hat{v}^{(k)}$ represents the normalized displacement increment ratio. Equation (11) shows that the criterion system established in this section is not a simple concatenation of multiple discrete results, but a unified compression of matrix spectrum, energy curvature and iterative convergence state into comparable numerical outputs.

The above criteria are output in the form of unified state vector in the program, and participate in the stability level discrimination of subsequent modules. Because the tensegrity structure has the characteristics of multi-configuration, multi-path and multi-prestress combination, only relying on the traditional linear determination will compress the sample difference, while the joint criterion can preserve the spectral variation, energy variation and solution process variation at the same time. In this way, the obtained state variables can not only reflect the stability properties of the structure under the current load step, but also describe its tendency to approach the instability boundary, providing learnable, comparable and traceable numerical inputs for the intelligent analysis module in Chapter III. The criterion system established in this section thus completes the transition from mechanical equilibrium to computational identification, and lays the foundation for multi-scheme stability comparison in subsequent experiments.

3 Construction of structural stability quantitative analysis model based on stiffness matrix calculation and intelligent analysis

3.1 Data mapping and stiffness matrix generation for tensegrity structures

The data mapping and stiffness matrix generation of tensegrity structures essentially organize joint coordinates, component connection relationships, material parameters, section properties, boundary constraints, initial prestresses and load paths into a unified calculation input. On this basis, degree-of-freedom expansion, element mapping, local matrix construction and global matrix assembly are completed. In this paper, the computational link of "parameter reading-topology analysis-degree of freedom numbering-element matrix generation-overall matrix assembly-feature cache" is adopted, so that the structural schemes under different configurations, different cable force distributions and different support conditions can form comparable matrix samples in the same data frame. Different from the modeling method that only serves for geometric display, the data mapping here is directly oriented to stiffness matrix calculation and subsequent stability quantitative analysis. Therefore, all design variables need to be unified coding, scale normalization and index binding before entering the numerical module.

In order to compress the geometric information, material information and constraint information of the cell layer into standard input vectors that can be directly called by the

program, this paper first defines the cell-level data mapping relationship as follows:

$$z_e = \Pi\left[x_i^T, x_j^T, \frac{x_j - x_i}{\|x_j - x_i\|_2}, L_e, E_e, A_e, T_e^0, c_i^T, c_j^T, \tau_e\right]^T \tag{12}$$

where x_i and x_j represent the node coordinates at both ends of the element, L_e represents the length of the element, E_e represents the elastic modulus, A_e represents the section area, T_e^0 represents the initial prestress, c_i and c_j represent the node constraint vector at both ends, τ_e represents the component category label, and Π represents the normalization and rearrangement operator. In Equation (12), the rod and cable are uniformly transcribed into data entries of the same dimension to provide consistent input for subsequent local stiffness generation.

Fig. 4 shows the data mapping and matrix generation process adopted in this section. The input on the left side of the figure includes node coordinates, rod-cable topology, material properties, boundary constraints, and prestress levels. In the middle part, topology analysis, local coordinate generation, degree of freedom numbering and unit mapping were completed in turn. On the right side, local stiffness construction, global assembly, matrix reduction, and feature caching are entered. The arrow line represents the one-way transformation from the design parameters to the stiffness matrix, and the dotted loop indicates that when the boundary condition or cable force level is changed, only the affected element is updated locally without recomputing all the samples. The process shows that the data mapping of tensegrity structure not only serves the matrix calculation itself, but also provides a uniform data entry for subsequent stability identification and scheme comparison.

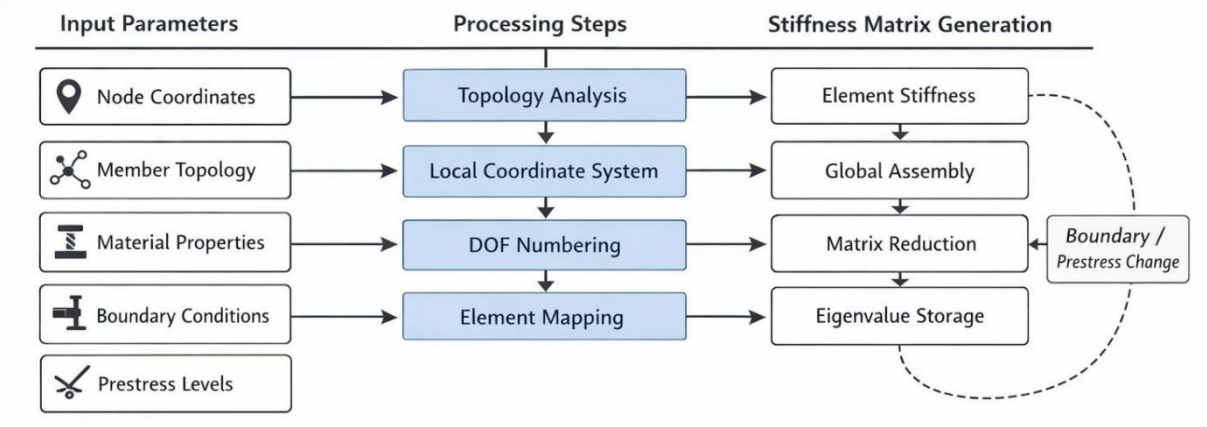

Figure 4: Flow chart of data mapping and stiffness matrix generation for tensegrity structures

In the program implementation, the set of nodes is saved as a three-dimensional coordinate array, and the connection relationship of components is represented by an edge table with attributes. The attribute fields include component type, material number, section parameters, initial cable force, length threshold and constraint label. Firstly, the sparse adjacency index is established according to the node number, and then the axial parameter table, prestress correction table and geometric mapping table are generated according to the category difference between the rod and cable. Through this process, the geometric adjustment in the structural design is no longer just a graphical change, but will be directly fed back to the matrix generation link, so as to ensure a consistent correspondence between the design parameters, the numerical analysis object and the stability characterization results.

In order to maintain the consistency of unit orientation, local basis and degree of freedom

mapping in the global coordinate system, this paper further defines the unit orientation basis and assembly mapping matrix as follows.

$$G_e = (e_i - e_j) \otimes I_3, \quad Q_e = [q_e, s_e, r_e], \quad R_e = Q_e^T G_e \tag{13}$$

where, e_i and e_j represent the node position basis vectors, I_3 is the third-order identity matrix, q_e represents the unit axial unit vector, s_e and r_e represent the orthogonal local basis vectors, R_e represents the mapping matrix from local degrees of freedom to global degrees of freedom. Equation (13) is used to ensure that the local stiffness template, geometric correction term and boundary additional term can be written into the overall system without ambiguity.

In order to ensure that the data mapping process has a uniform interface, this paper organizes nodes, components, constraints and loads into four main tables, and establishes key index in the script. The node table holds the number, coordinates, degrees of freedom status and level labels. The component table saves the endpoint index, component category, section size, material parameters and initial cable force. The constraint table records the support type, direction limit and elastic boundary coefficient. The load table records the external force path, disturbance labels, and additional load parameters. Table 1 presents the data field organization adopted in this section. In this structured way, parameter reading, filtering, rearrangement, assembly, and caching can all be done automatically by the program, thus providing a stable entry point for batch matrix generation.

Table 1: Tensegrity structure data mapping field organization table

Data Table	Main Fields	Field Meaning	Output Object
Node Table	NodeID, X, Y, Z, DOFTag, LayerTag	Node position and degree-of-freedom status	Node coordinate matrix, degree-of-freedom index
Element Table	ElementID, StartID, EndID, Type, E, A, T0	Element connectivity, material properties, section parameters, and prestress	Element attribute vector, local direction basis
Constraint Table	ConstraintID, NodeID, UX, UY, UZ, RX, RY, RZ, Kb	Support direction constraints and elastic boundary coefficients	Constraint matrix, penalty block
Load Table	LoadID, NodeID, PathTag, Fx, Fy, Fz, DisturbTag	External load path and disturbance labels	Load vector, sample labels

After obtaining the node, member, and constraint data, the program generates unit layer reinforcement stiffness based on geometric length, direction vector, prestressed state, and member type. Considering that prestress and configuration coupling have a direct impact on global stability in tensegritic structures, the local matrix does not adopt a single axial stiffness form, but writes material stiffness, geometric correction and configuration coupling into the local expression together. Its reinforcement stiffness is defined as follows.

$$\widetilde{K}_e = \frac{E_e A_e}{L_e} R_e^T M_a R_e + \frac{T_e^0}{L_e} R_e^T M_g R_e + \xi_e R_e^T M_c R_e \tag{14}$$

Here, M_a represents the material stiffness template matrix, M_g represents the geometric correction template matrix, M_c represents the configuration coupling template matrix, and

ξ_e represents the configuration coupling coefficient. Equation (14) shows that the local element stiffness is simultaneously affected by the material, cable force and configuration organization.

Fig. 5 illustrates the program execution logic of the matrix generation phase. The input side first reads the node table, component table and constraint table, and then calculates the length, orientation and local base by the parser, and then constructs the enhanced stiffness by the local matrix generator, and then writes the overall matrix by the sparse assembler. The constraint merging module unifies the encoding of fixed, articulated and elastic supports into boundary correction blocks, and synchronously generates matrix labels, sample numbers and configuration labels at the final output. This process extends the matrix generation from a single solution to a traceable, cacheable, and batchable procedural link.

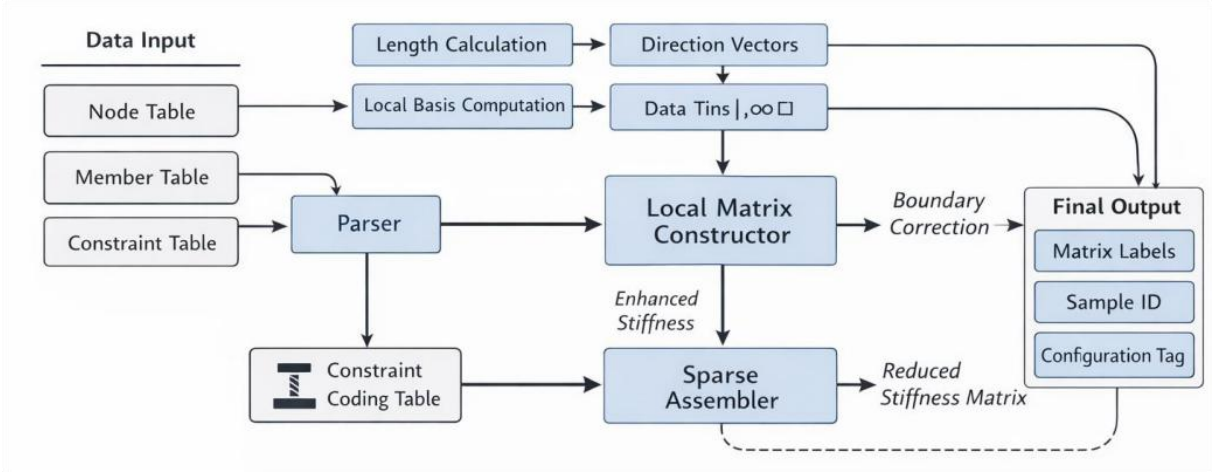

Figure 5: Program execution logic diagram for the stiffness matrix generation phase

In order to write the enhanced stiffness of each element into the overall system and retain the additional influence caused by boundary constraints, the overall initial assembly relationship is expressed as follows.

$$K^{(0)} = \sum_{e=1}^{m} P_e^T \tilde{K}_e P_e + \lambda_b B^T \Omega B \tag{15}$$

Here, m represents the total number of cells, P_e represents the cell assembly matrix, B represents the boundary mapping matrix, Ω represents the boundary weight matrix, and λ_b represents the boundary correction coefficient. Equation (15) unifies the element layer stiffness, the overall assembly relationship and the boundary constraints into a sparse matrix expression.

In order to weaken the interference of constrained degrees of freedom on subsequent spectrum analysis and sample comparison, this paper further implements constrained elimination of the overall matrix, and its reduction relation is written as follows.

$$K_r = K_{ff} - K_{fc}(K_{cc} + \mu I)^{-1} K_{cf} \tag{16}$$

Here, K_{ff} represents the free free block matrix, K_{fc} and K_{cf} represent the free constraint coupling block matrix, K_{cc} represents the constraint constraint block matrix, and μ represents the stabilization coefficient. Equation (16) ensures that the stiffness matrix samples formed under different boundary conditions are still uniformly comparable.

In order to make the reduced matrix object directly enter the subsequent intelligent analysis module, this paper further translates it into a unified dimension cache vector, which is defined as follows:

$$y = \left[\log\det(K_r + \varepsilon I), \kappa_2(K_r), \rho_{nz}(K_r), \frac{\sum_{i=1}^{p}\lambda_i}{\sum_{j=1}^{n}\lambda_j}, \|K_r\|_F, \zeta\right]^T \tag{17}$$

Here, ε is the regularization constant, $\kappa_2(K_r)$ represents the two-norm condition number, $\rho_{nz}(K_r)$ represents the nonzero element density, λ_i represents the matrix eigenvalue,$\|K_r\|_F$ represents the Frobenius norm, and ζ represents the combination term of configuration label and load label. Equation (17) compreses the output of the matrix layer into uniform sample entries to facilitate subsequent stability level identification and batch comparison.

In order to ensure data consistency in batch processing scenario, the program executes three types of checks synchronously after matrix generation. The first type of check is oriented to topology closure, which checks node degree, endpoint coincidence error and isolated edge label. The second type of check is oriented to the integrity of degrees of freedom, and the constrained direction, release direction and elastic support coefficient are uniformly sorted out. The third type of verification is oriented to sample archiving, which automatically verifies matrix dimension, sparsity rate, label integrity and feature vector length. After these processes, data mapping and stiffness matrix generation are no longer just pre-processing steps, but become the core data interface connecting structural design, numerical solution and intelligent analysis.

3.2 Structural stability quantitative analysis module based on stiffness matrix feature calculation

This module does not perform the full finite element solution repeatedly, but based on the matrix samples generated in Section 3.1, extracts the key variables that can characterize the stability margin, configuration coupling strength, and boundary sensitivity, and organizes them into trainable, comparable, and writeback analysis elements. The module inputs include the reduced stiffness matrix, the eigenvalue sequence, the boundary label, the prestress label and the load path label, and the output includes the stability margin estimate, the state class probability and the sensitive component ranking result. After this process, multiple sets of tensegrity design schemes can first complete matrix feature screening, and then perform fine calculation on critical samples, thus connecting numerical analysis and design decision as a continuous link.

In the feature organization stage, the program performs spectral decomposition, statistical transformation and scale normalization on the reduced stiffness matrix, and then writes the minimum positive eigenvalue, condition number, energy curvature, sparse density, principal minor change rate and prestress gradient into a unified vector. Since the matrix size of different configurations is not consistent, the module uses block pooling and length mapping strategies to compress the matrix statistics of different dimensions to a fixed input scale, and retains the local response information of the node layer and component layer. In order to avoid the high correlation index repeatedly entering the subsequent network, the script synchronously performs correlation screening and variance filtering, and only retains the variables that contribute to the stable rank discrimination. After this process, the matrix object is transformed into a compact representation which preserves the mechanical meaning and is suitable for program invocation.

Table 2 shows the main input and output organization of the quantitative analysis module.

The matrix layer features are responsible for describing the global stiffness state, the component layer features are responsible for characterizing the local disturbance propagation path, and the label layer holds the load step, boundary type, and stability level. The three classes of information are read synchronously in the same batch, enabling regression estimation, classification judgment, and sensitivity ranking to share intermediate features. This structure not only ensures the one-to-one correspondence between the analysis results and the original matrix object, but also facilitates the ablation comparison and error tracking in the subsequent experimental stage.

Table 2: Module organization table for quantitative analysis of structural stability based on stiffness matrix feature calculation

Level	Input Content	Processing Method	Output Result
Matrix Layer	Reduced stiffness matrix, eigenvalue sequence, condition number, curvature indicators	Normalization, block pooling, gated weighting	Principal feature vector
Element Layer	Local element stiffness, prestress gradient, adjacency relations	Adjacency propagation, local aggregation	Local response features
Decision Layer	Principal feature vector, local response features, boundary labels	Regression estimation, three-class classification, sensitivity ranking	Margin value, state probabilities, ranking list

In order to map the multi-source matrix statistics into a unified principal eigenvector, the module first constructs the input representation as follows.

$$\mathrm{h}^{(0)} = \mathrm{Norm}\left[\log(\Lambda_{\min}^{+} + \varepsilon), \log \kappa(\mathrm{K_r}), \chi, \rho_{\mathrm{nz}}(\mathrm{K_r}), \Delta_{\det}, \nabla_{\mathrm{p}}, \mathrm{b}, \mathrm{l}\right]^{\mathrm{T}} \tag{18}$$

Here, $\Lambda_{\min}^{+}$ represents the smallest positive eigenvalue, $\kappa(\mathrm{K_r})$ represents the condition number of the reduced stiffness matrix $\mathrm{K_r}$, χ represents the energy curvature index, $\rho_{\mathrm{nz}}(\mathrm{K_r})$ represents the nonzero element density, $\Delta_{\det}$ represents the rate of change of the principal minor, ∇_{p} represents the prestress gradient, b and l represent the boundary label and load label, respectively, and $\mathrm{Norm}(\cdot)$ represents the normalized operator. Equation (18) compresses the spectral information, boundary information and load information into a unified input vector, so that statistics from different sources maintain comparable scales.

In order to suppress noisy statistical terms and increase the expression weight of sensitive variables in the main feature extraction layer, the module further adopts gated fusion relationship as follows:

$$\mathrm{g} = \sigma\left(\mathrm{W_g h}^{(0)} + \mathrm{b_g}\right), \quad \mathrm{h_m} = \mathrm{g} \odot \tanh\left(\mathrm{W_m h}^{(0)} + \mathrm{b_m}\right) + (1 - \mathrm{g}) \odot \mathrm{h}^{(0)} \tag{19}$$

Here, g represents the gating weight vector, $\sigma(\cdot)$ represents the Sigmoid function, $\mathrm{W_g}$ and $\mathrm{W_m}$ are trainable weight matrices, $\mathrm{b_g}$ and $\mathrm{b_m}$ are bias vectors, $\odot$ represents Hadamard product, and $\mathrm{h_m}$ represents the fused main feature. Equation (19) enables the module to automatically reduce the interference of the noise term on the subsequent judgment while retaining the original mechanical characteristics.

In order to propagate the local response of the component layer to the global representation along the force path, this paper uses the adjacency aggregation with attention

weight to express as follows:

$$\alpha_{ij}^{(t)} = \frac{\exp\left(a^{T}\left[Uh_i^{(t)} \,\|\, Uh_j^{(t)}\right]\right)}{\sum_{k\in\mathcal{N}(i)}\exp\left(a^{T}\left[Uh_i^{(t)} \,\|\, Uh_k^{(t)}\right]\right)}, \quad h_i^{(t+1)} = \sum_{j\in\mathcal{N}(i)} \alpha_{ij}^{(t)}\, Uh_j^{(t)} \tag{20}$$

Here, $\alpha_{ij}^{(t)}$ represents the attention weight of node j to node i in round t of propagation, $\mathcal{N}(i)$ represents the adjacency set of node i, U is the linear transformation matrix, a is the attention parameter vector, and $\|$ represents vector concatenation. Equation (20) diffuses the local matrix sensitivity into the global representation along the force path, thus enhancing the influence of the sensitive components on the overall stability level.

In the regression branch, the module takes the stability margin as a continuous output and couples the global features with the local propagation features through the bilinear mapping. The regression branch gives continuous values instead of only outputting discrete states, and is therefore suitable for performing ranking, threshold control, and scheme priority assignment during the design sieving phase. In the classification branch, the module outputs three types of states, stable, critical and unstable, and uses the shared principal features to form joint constraints with the regression branch. With this definition, the discrete state judgment and the continuous margin estimation can be consistent in the same feature space.

In order to output the stability margin and the three-class state probabilities simultaneously, the module maps the shared features into two branches, regression and classification, which are expressed as follows:

$$\hat{\eta} = h_m^{T} W_r \bar{h} + u^{T} h_m + c, \quad p = \mathrm{SoftMax}\left(W_c\left[h_m \| \bar{h} \| \hat{\eta}\right] + b_c\right) \tag{21}$$

where $\hat{\eta}$ represents the stability margin prediction value, $\bar{h}$ represents the global and local joint features after propagation, W_r represents the bilinear regression kernel, u and c are regression parameters, p represents the probability vectors of stable, critical and unstable states, W_c and b_c are classification weights and biases. Equation (21) unitizes the continuous estimation and discrete judgment into the same feature space, so that the ranking of alternatives is consistent with the state judgment.

In order to ensure the stable execution of the module in batch processing scenarios, the program uses matrix cache and asynchronous reading to manage samples. Each batch of data is checked by spectral statistics, label integrity and outlier shielding before entering the calculation graph, and then sent to the shared front-end in the form of tensor. The front-end parameters are jointly called by the regression branch and the classification branch, thereby reducing the recomputation overhead and maintaining numerical consistency between different outputs. This mechanism enables the module not only to serve the off-line training, but also to support the rapid review in the design phase. At the same time, the ranking results of sensitive components are synchronously bound with the node number and the component number, which facilitates the subsequent location of local instability propagation links and provides a direct basis for the modification of structural parameters. The output thus formed has not only predictive but also clear engineering interpretation value.

4 Experiment and result analysis

In order to verify the effectiveness of the stiffness matrix feature calculation method in the quantitative analysis of the stability of tensegrity structures, this paper carried out

comparative experiments, ablation experiments and visualization analysis on the self-built sample set. The sample set contains a total of 3600 sets of parameterized configurations covering the main design variables such as rod-cable length ratio, prestress level, boundary combination, and load path. All samples were divided into training set, validation set and test set according to 7∶2∶1, and matrix generation, feature extraction and state determination were completed in the same hardware environment. The evaluation metrics are classification accuracy, F1 score, mean absolute error of stability margin, and inference time for one sample.

Table 3 presents the overall performance comparison of different methods on the test set. Baseline-MLP only maps the statistical features in a plane, which is difficult to maintain the correspondence between the matrix spectral information and the local coupling relationship. The accuracy is 90.8%, the F1 value is 0.871, and the mean absolute error of stability margin is 0.061. After introducing adjacency propagation into GCN-Transformer, the accuracy is improved to 93.2%, the F1 value reaches 0.897, and the error is reduced to 0.046. The proposed method jointly uses spectral features, boundary labels and local propagation information, and the accuracy reaches 95.4%, the F1 value is 0.918, the mean absolute error of stability margin is controlled at 0.037, and the inference time for a single sample is 0.42 s. Compared with the baseline process that only relies on numerical screening, the overall computation time is reduced by 21.6%, indicating that the stiffness matrix features have high information density in the fast discrimination stage.

Table 3: Overall performance comparison of different methods

Method	Accuracy / %	F1 Score	Stability Margin MAE	Single-Sample Inference Time / s
Baseline-MLP	90.8	0.871	0.061	0.53
GCN-Transformer	93.2	0.897	0.046	0.48
Proposed Method	95.4	0.918	0.037	0.42

Fig. 6 illustrates the evolution curve of the minimum positive eigenvalue along the load path for different prestress levels. The low prestressed samples showed a significant decrease near the load step 0.74, the medium prestressed samples entered the slow decrease zone near 0.81, and the high prestressed samples maintained a high eigenvalue level before 0.88. The judgment of the state switching position of the three types of samples is basically consistent with the numerical calculation results, and the inflection point from stable to critical can be stably identified especially in the middle and later load interval. This indicates that the spectral change of the stiffness matrix has a high identification of the stability boundary, and the level of prestress will directly change the spectral decay rate when approaching instability.

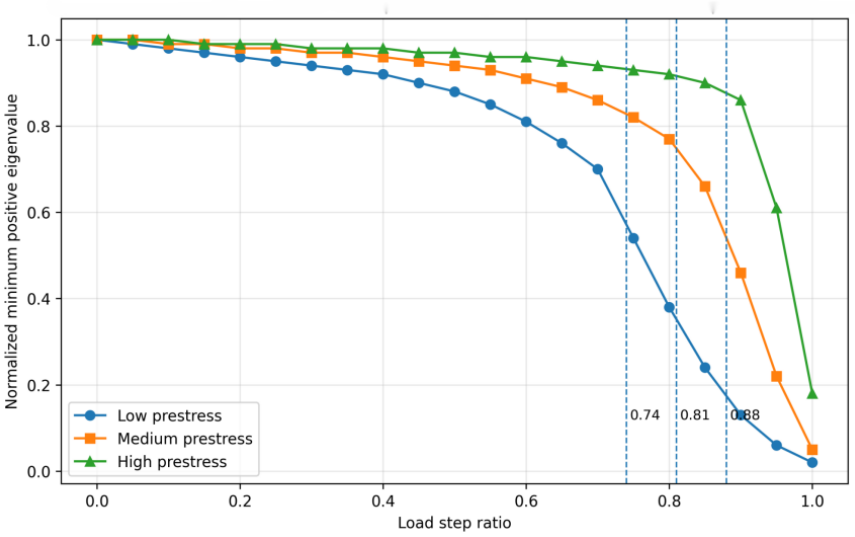

Figure 6: Minimum positive eigenvalue evolution curves for different prestress levels

To further observe the distribution of classification results, Fig. 7 shows the confusion matrix heatmap of the three class states of the test set. The recognition rate of stable state, critical state and unstable state is 96.1%, 93.8% and 96.4%, respectively. A small number of critical samples were judged as stable, mainly concentrated in the interval where the boundary release was weak and the curvature change was not fully expanded. A small number of critical samples were judged to be unstable, which corresponded to the instantaneous amplification caused by the sudden drop of local member stiffness. On the whole, the proportion of the main diagonal area of the heat map is significantly higher than that of the off-diagonal area, indicating that the proposed method has a relatively clear division boundary for the three types of states.

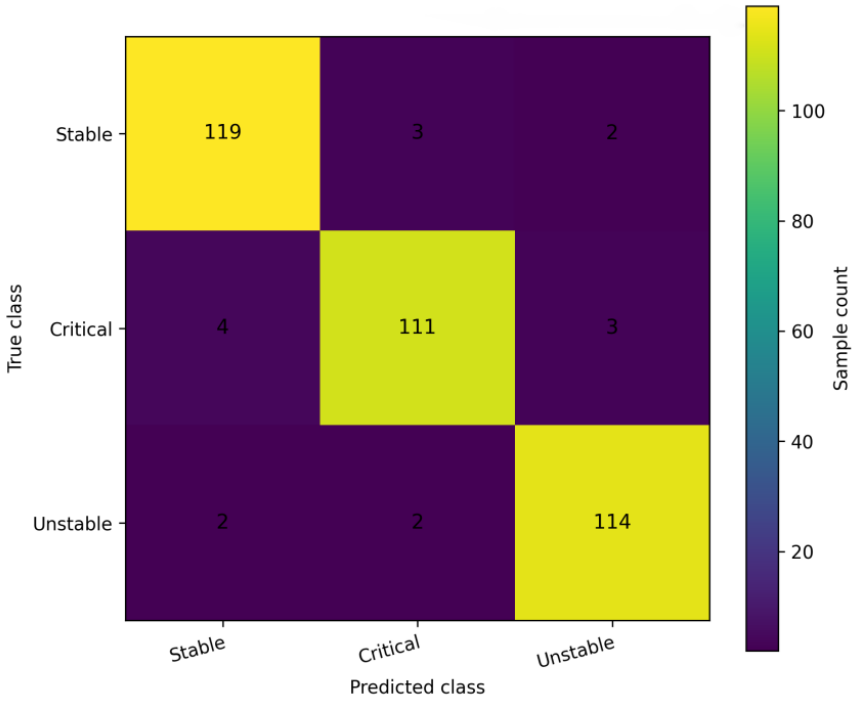

Figure 7: Heatmap of the steady-state confusion matrix for the test set

Table 4 presents the results of ablation experiments. After removing the spectral features, the accuracy decreases to 92.6%, and the F1 value decreases to 0.889, which indicates that the minimum positive eigenvalue, the condition number and the change rate of the principal minor are still the backbone information for the overall stability judgment. After removing the local propagation, the mean absolute error of the stability margin increases to 0.051, indicating that the lack of local component perturbation information can weaken the identification of sensitive paths. After removing boundary labels, the recall of critical states decreases most obviously, indicating that boundary conditions have a direct impact on the position of state switching. The complete module remains optimal in all four indicators, which proves that there is a relatively stable synergistic relationship between the shared front end, local propagation and label constraints.

Table 4: Results of ablation experiments

Model Configuration	Accuracy / %	F1 Score	Stability Margin MAE	Critical-State Recall / %
Full Module	95.4	0.918	0.037	94.6
Without Spectral Features	92.6	0.889	0.049	90.8
Without Local Propagation	93.1	0.894	0.051	91.7
Without Boundary Labels	93.4	0.901	0.044	89.9

Fig. 8 shows a scatter comparison between the predicted stability margin and the numerical results. There were 360 groups of samples in the test set. The Pearson correlation coefficient between the predicted value and the numerical results was 0.964, the determination coefficient R^2 was 0.942, the mean absolute error was 0.037, and the root mean square error was 0.049. The average deviation of the high margin interval is controlled within 0.018, the transition interval is 0.031, and the critical adjacent interval is 0.056. A total of 302 groups of samples had absolute deviation less than 0.04, accounting for 83.9% of the test set, indicating that the method has a good continuous prediction ability for stability margin.

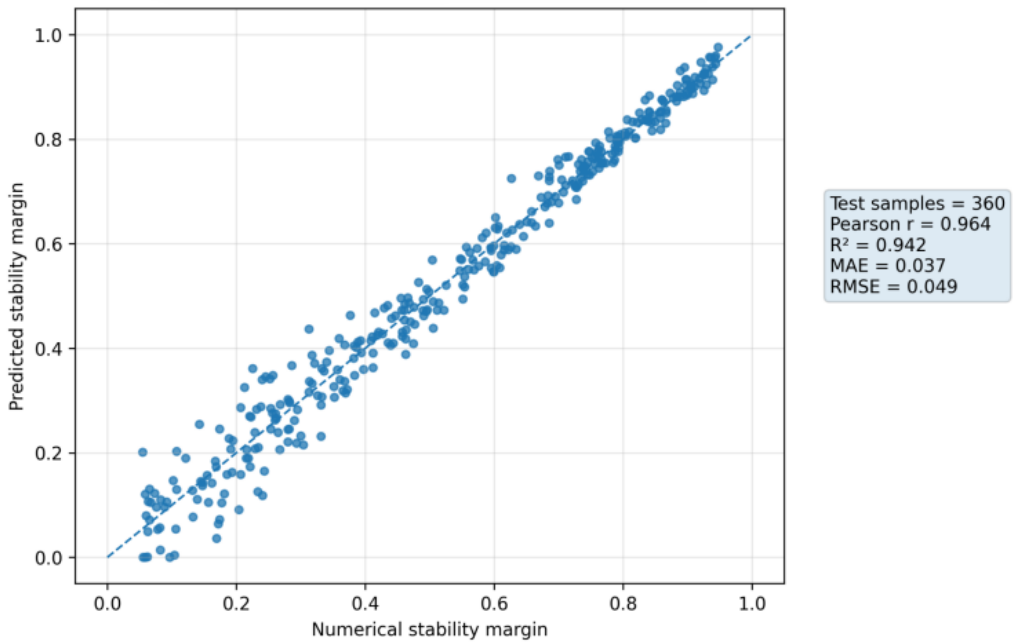

Figure 8: Scatter plot of predicted stability margin versus numerical results

Fig. 9 further demonstrates the distribution of the stability margin box line for the samples of four types of typical configurations, where 40 groups of samples are taken for each type of configuration. The median stability margin is 0.81 for the triangular prism configuration, 0.72 for the symmetric extension configuration, 0.68 for the mixed support configuration, and 0.59 for the cable net extension configuration. The corresponding variances are 0.0064, 0.0081, 0.0057 and 0.0149, respectively. Among them, the dispersion of the cable net expansion configuration is the largest, and the number of outliers is 5, indicating that this type of configuration is more sensitive to boundary changes and prestress disturbances. The results of box line distribution show that different topological organization methods will directly affect the distribution range and central tendency of stability margin.

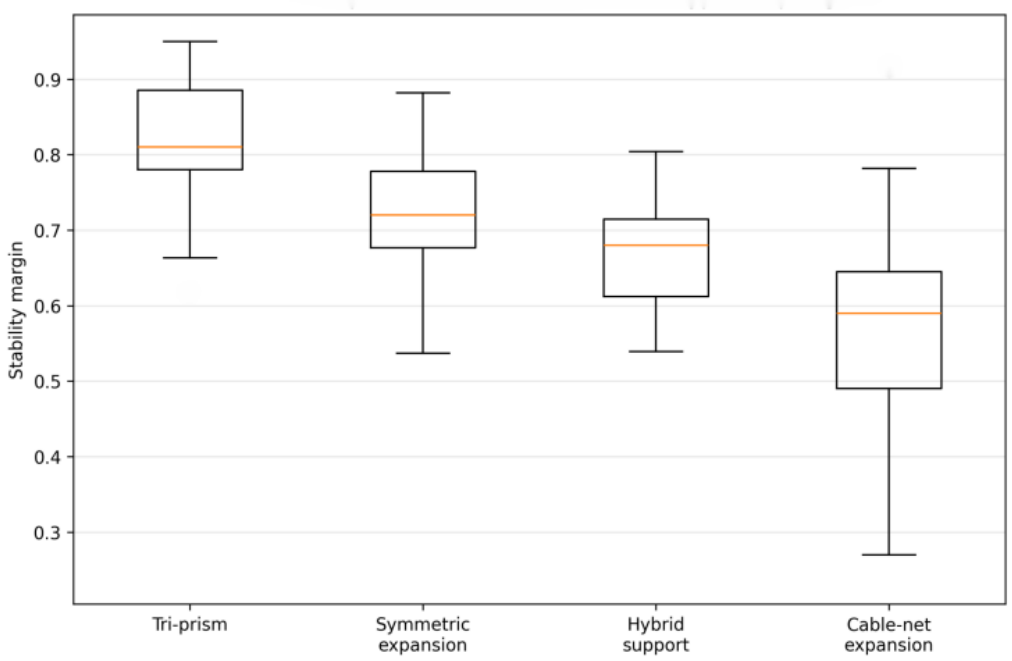

Figure 9: Box plots of stability margin distribution for samples of different configurations

Taking the above results together, the stiffness matrix feature calculation method shows good engineering adaptability in tensegrity structure design scenarios. This method can translate the matrix spectrum, local coupling and boundary information into computable output, so that the design sample can complete the stability screening before entering the fine solution. After comparing the test results under the condition of multiple configurations and multiple parameters, it can be seen that the proposed method maintains a relatively balanced performance among recognition accuracy, margin error and reasoning efficiency, and has a relatively stable tracking ability for the state change of the critical interval.

5 Conclusion

This study focuses on the influence of stiffness matrix on structural stability in tensegrity structure design, and combines parametric modeling, matrix generation, spectral feature extraction and intelligent discrimination processes to form a stability margin estimation and state recognition framework. Through theoretical derivation, implementation and sample verification, the multi-configuration comparison and fast screening links are formed, which show that the stiffness matrix is not only the intermediate object of structural response

solution, but also an important data carrier for stability analysis and design decision.

(1) In the stage of model construction, the mapping from geometric parameters, topological relations, boundary constraints to global stiffness matrix of tensegrity is completed. Local matrix, global assembly and feature caching mechanisms are established, and design variables can be directly entered into numerical analysis. The test results show that the state recognition accuracy of the proposed method on the test set reaches 95.4%, and the F1 value is 0.918, which indicates that the matrix spectral features and local propagation information can effectively support the stable state division.

(2) For stability margin prediction, we construct a stiffness matrix feature joint analysis module, which organizes the minimum positive eigenvalue, condition number, energy curvature and boundary label into a unified input term. The results show that the predicted mean absolute error of stability margin is 0.037, and the coefficient of determination is 0.942, which indicates that the module can maintain the consistency between the numerical results and the predicted results, and realize the continuous comparison of multiple configurations.

(3) In terms of engineering suitability, the proposed method connects matrix generation, feature extraction and state discrimination into a unified process, so that the design samples can be quickly screened before entering the detailed calculation. Compared with the baseline process, the single sample inference time is reduced by 21.6%, which shows that the proposed method has good computational efficiency and batch processing ability while maintaining the analysis accuracy.

There are still limitations to this study. The samples are mainly from the parametric generated data, and the coverage of the measured engineering data is still limited. Although the configuration contains a variety of topologies, it is still extensible to express complex boundary disturbances and nonlinear material states. The current module focuses on off-line analysis and has not yet been incorporated into real-time writeback. Subsequent research can introduce measured data, enhance the ability of cross-configuration migration, and add online update and lightweight deployment mechanisms to further improve the generalization ability, interpretation ability, and application depth of the model in complex design scenarios.

References

[1] Ma S, Chen M, Skelton R E. Dynamics and control of clustered tensegrity systems[J]. Engineering Structures, 2022, 264: 114391.

[2] Lee S, Lieu Q X, Vo T P, et al. Deep neural networks for form-finding of tensegrity structures[J]. Mathematics, 2022, 10(11): 1822.

[3] Koohestani K. Novel topological and geometrical modelling of N-frequency geodesic icosahedron tensegrities[J]. Engineering with Computers, 2022, 38(6): 5733-5745.

[4] Bel Hadj Ali N, Aloui O, Rhode-Barbarigos L. A finite element formulation for clustered cables with sliding-induced friction[J]. International Journal of Space Structures, 2022, 37(2): 81-93.

[5] Song K, Scarpa F, Schenk M. Form-finding of tessellated tensegrity structures[J]. Engineering Structures, 2022, 252: 113627.

[6] Xu X, Huang S, Shu T, et al. A novel two-step tensegrity topology-finding method based on mixed integer programming and nonlinear programming[J]. International Journal of Steel Structures, 2022, 22(4): 1266-1282.

[7] Fernández-Ruiz M A, Hernández-Montes E, Gil-Martín L M. Topological design of the octahedron tensegrity family[J]. Engineering Structures, 2022, 259: 114211.

[8] Trinh D T N, Lee S, Kang J, et al. Force density-informed neural network for prestress design of tensegrity structures with multiple self-stress modes[J]. European Journal of Mechanics-A/Solids, 2022, 94: 104584.

[9] Zhang N, Luo B, Liu H, et al. Prestress self-equilibrium force-finding method for cable-supported grid structures considering zero-stress state form-finding and the construction process[J]. Buildings, 2022, 12(6): 749.

[10] Obara P, Tomasik J. Dynamic Stability of Tensegrity Structures—Part I: The Time-Independent External Load[J]. Materials, 2023, 16(2): 580.

[11] Chen M, Bai X, Skelton R E. Minimal mass design of clustered tensegrity structures[J]. Computer Methods in Applied Mechanics and Engineering, 2023, 404: 115832.

[12] Chen M, Fraddosio A, Micheletti A, et al. Analysis of clustered cable-actuation strategies of V-Expander tensegrity structures[J]. Engineering Structures, 2023, 296: 116868.

[13] Ge Y, He Z, Li S, et al. A machine learning-based probabilistic computational framework for uncertainty quantification of actuation of clustered tensegrity structures[J]. Computational Mechanics, 2023, 72(3): 431-450.

[14] Kumar S, Aswal N, Sen S. A novel Genetic algorithm based form-finding approach towards the improved design of tensegrity utility bridge[C]//Structures. Elsevier, 2023, 58: 105401.

[15] Luo A, Cao Z, Liu H, et al. Stiffness of three-bar tensegrity structure[J]. Engineering Computations, 2023, 40(4): 823-835.

[16] Feng X, Fan Y, Peng H, et al. Optimal active vibration control of tensegrity structures using fast model predictive control strategy[J]. Structural Control and Health Monitoring, 2023, 2023(1): 2076738.

[17] Wang Y, Xu X, Luo Y. Self-equilibrium, mechanism stiffness, and self-stress design of general tensegrity with rigid bodies or supports: A unified analysis approach[J]. Journal of Applied Mechanics, 2023, 90(8): 081004.

[18] Xu X, Huang S, Wang Y, et al. A generalized objective function based on weight coefficient for topology-finding of tensegrity structures[J]. Applied Mathematical Modelling, 2023, 115: 541-567.

[19] Liu H, Sanaullah, Vumiliya A, et al. A resource-efficient form-finding approach to tensegrity structures[J]. Engineering Computations, 2024, 41(1): 1-17.

[20] Wang Y, Han Z, Xu X, et al. Topology optimization of active tensegrity structures[J]. Computers & Structures, 2024, 305: 107513.